Chapter 1
Enhancement of the Faraday and Other Magneto-Optical Effects in Magnetophotonic Crystals

A.P. Vinogradov, A.V. Dorofeenko, A.M. Merzlikin, Y.M. Strelniker, A.A. Lisyansky, A.B. Granovsky, and D.J. Bergman

Abstract It is shown that for existent natural materials the Faraday rotation is far below the theoretical limit [Steel et al. in J. Lightwave Technol. 18:1297, 2000]. Under this condition the value of the Faraday rotation is primarily determined by the Q-factor, while the low group velocity value, multipass traveling and energy concentration in magneto-optical material play a secondary role. A comparative analysis of the efficiency of different schemes employing defect modes, Tamm surface states, the Borrmann effect and plasmon resonance is presented.

1.1 Introduction

Magneto-optical (MO) effects have been known since 1846 when Faraday discovered a rotation of the polarization of a linearly polarized electromagnetic wave traveling through a slab of a gyrotropic substance placed in a static magnetic field. It is also known that Faraday and other MO effects can be essentially enhanced

A.P. Vinogradov (✉) · A.V. Dorofeenko · A.M. Merzlikin
Institute for Theoretical and Applied Electromagnetics RAS (ITAE RAS), Moscow 125412, Russia
e-mail: A-Vinogr@yandex.ru

A.P. Vinogradov · A.V. Dorofeenko
Moscow Institute of Physics and Technology, Dolgoprudniy, Moscow Reg. 141700, Russia

Y.M. Strelniker
Department of Physics, Bar-Ilan University, Ramat-Gan, Israel

A.A. Lisyansky
Physics Department, Queens College of the City University of New York, Flushing, NY 11367, USA

A.B. Granovsky
Faculty of Physics, M.V. Lomonosov Moscow State University, Moscow 119991, Russia

D.J. Bergman
School of Physics and Astronomy, Tel Aviv University, Tel Aviv 69978, Israel

M. Inoue et al. (eds.), *Magnetophotonics*, Springer Series in Materials Science 178,
DOI 10.1007/978-3-642-35509-7_1,

in the presence of a resonance. One such resonance, which is currently under intensive study, is the surface plasmon resonance [1]. It is commonly believed that this or similar resonances are responsible for the Extraordinary Light Transmission (ELT) through a metal film, perforated by a periodic array of sub-wavelength holes [2, 3], as well for other new phenomena recently found in photonic crystals with bandgaps [4–6]. Application of a static magnetic field to such systems induces strong optical and transport anisotropy, leads to appearance of additional off-diagonal tensor components in the effective permittivity tensor $\hat{\varepsilon}$ and changes the surface plasmon frequency [7–13]. Therefore, the application of a static magnetic field to conducting systems with dielectric islands or to dielectric systems with metallic islands, as well the introduction of gyrotropic inclusions into photonic crystals [4, 14–17] should lead to the appearance of strong MO effects [18–23] and to possibilities for manipulation of light propagation [7–13, 24–33].

Enhancements of the Faraday and Kerr effects was demonstrated in one-dimensional MO quasicrystals [34], in systems with a random distribution of MO layers [35], in magnetophotonic crystals (MPC's) [6], in MPC's with one or two defects [36–40], and in a system of two adjoined PC's including MO layers and having an optical Tamm state [4, 5, 16]. At the present time, microscopic mechanisms of MO phenomena are well studied [41]. They are caused by the spin-orbit interaction at inter- and intraband optical transitions. Although, MO phenomena are weak, like all relativistic effects, they can be substantially enhanced by using MPCs. Below we discuss the physical phenomena underlying such an enhancement.

While the very fact of enhancement of MO effects in multilayer structures has been known for a long time [42, 43], the mechanism which leads to this enhancement is still under discussion. In some papers [36, 44, 45], the origin of the enhancement is attributed to the fact that the light localized near a defect has an increased optical path length, which results in the increase of the Faraday rotation, similar to the classical Faraday experiment. The authors of Refs. [46, 47] consider the low group velocity, which increases the time of interaction of light with matter, as the cause of the enhancement.

Considerable understanding was achieved in Ref. [36], where the role of the phase change in the vicinity of a resonance was shown, the decrease of the transmission with the growth of the Faraday rotation was explained and a two-defect scheme, providing high transmission at large Faraday rotation, was suggested.

In the present chapter, we theoretically predict the phase shift of π, provided naturally by the resonance, causes a giant increase of the Faraday angle from the small bulk value, determined by the MO constant, to a large value close to $\pi/2$. If the splitting of the resonance for the right and left circular polarizations is small, the Faraday effect is shown to be proportional to the Q-factor of the resonance and to the field confinement factor. If the splitting is not small, the signal amplitude inevitably decreases with the increase of the Faraday angle. To avoid this shortcoming, a structure using resonances of different orders is suggested, in principle providing the maximum Faraday rotation of $\pi/2$ at the transmission equal to unity.

1.2 Voigt Configuration

MO effects in metamaterial and magnetophotonic crystals should be calculated using proper formulas written in general form without making any assumptions and simplifications which could be correct for natural materials but not valid for artificial metamaterials. As was shown in Refs. [7–12], an application of a static magnetic field to metamaterials (see Fig. 1.1) can lead to magneto-induced anisotropy and to the appearance of additional off-diagonal terms in the electric permittivity and magnetic permeability tensors. Here we only briefly outline their derivation, referring the reader to Refs. [48–56] for more details.

We are looking for a solution to Maxwell's equations in the form of a monochromatic plane wave with the frequency ω propagating along the y-axis, with electric and magnetic fields $E = E_0 \exp(-i\omega t + i\mathbf{k}\cdot\mathbf{r})$ and $H = H_0 \exp(-i\omega t + i\mathbf{k}\cdot\mathbf{r})$, respectively. Here $\mathbf{E}_0$ and $\mathbf{H}_0$ are constant amplitudes and $\mathbf{k} \equiv (0, k, 0)$ is the wavevector in the y-direction. Substituting this into Maxwell's equations we obtain

$$k^2\mathbf{E}_0 - \mathbf{k}(\mathbf{E}_0\cdot\mathbf{k}) = \left(\frac{c}{\omega}\right)^2 \hat{\varepsilon}\mathbf{E}_0, \tag{1.1}$$

where $\hat{\varepsilon}$ is the electric permittivity tensor of the considered metamaterial and $\mathbf{k}$ is a complex wavevector.

For the vector directions shown in Fig. 1.1, (1.1) takes the form

$$\begin{aligned}
&\left[\left(\frac{c}{\omega}\right)^2 k^2 - \varepsilon_{xx} + \frac{\varepsilon_{xy}\varepsilon_{yx}}{\varepsilon_{yy}}\right]E_x - \left(\varepsilon_{xz} - \frac{\varepsilon_{xy}\varepsilon_{yz}}{\varepsilon_{yy}}\right)E_z = 0,\\
&-\left(\varepsilon_{zx} - \frac{\varepsilon_{zy}\varepsilon_{yx}}{\varepsilon_{yy}}\right)E_x + \left[\left(\frac{c}{\omega}\right)^2 k^2 - \varepsilon_{zz} + \frac{\varepsilon_{zy}\varepsilon_{yz}}{\varepsilon_{yy}}\right]E_z = 0.
\end{aligned} \tag{1.2}$$

These equations have a solution only if their determinant vanishes. This gives the following values for the wavevectors $k_\pm$:

$$\begin{aligned}
N_\pm^2 &\equiv \left(\frac{c}{\omega}\right)^2 k_\pm^2\\
&= \frac{1}{2}\left(\varepsilon_{xx} + \varepsilon_{zz} - \frac{\varepsilon_{zy}\varepsilon_{yz}}{\varepsilon_{yy}} - \frac{\varepsilon_{xy}\varepsilon_{yx}}{\varepsilon_{yy}}\right)\\
&\quad \pm \left[\frac{1}{4}\left(\varepsilon_{xx} + \varepsilon_{zz} - \frac{\varepsilon_{zy}\varepsilon_{yz}}{\varepsilon_{yy}} - \frac{\varepsilon_{xy}\varepsilon_{yx}}{\varepsilon_{yy}}\right)^2 - \left(\varepsilon_{xx} - \frac{\varepsilon_{xy}\varepsilon_{yx}}{\varepsilon_{yy}}\right)\left(\varepsilon_{zz} - \frac{\varepsilon_{zy}\varepsilon_{yz}}{\varepsilon_{yy}}\right)\right.\\
&\quad \left. + \left(\varepsilon_{xz} - \frac{\varepsilon_{xy}\varepsilon_{yx}}{\varepsilon_{yy}}\right)\left(\varepsilon_{zx} - \frac{\varepsilon_{zy}\varepsilon_{yx}}{\varepsilon_{yy}}\right)\right]^{1/2}.
\end{aligned} \tag{1.3}$$

Thus, there are four solutions to (1.1): two of them represent forward propagating waves with $k_\pm = \sqrt{N_\pm^2}\omega/c$ while the other two represent backward propagating waves with $k_\pm = -\sqrt{N_\pm^2}\omega/c$. Therefore, a plane-polarized wave normally incident

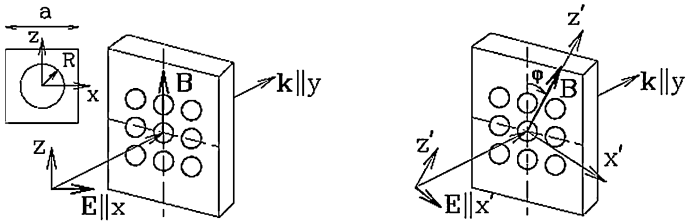

Fig. 1.1 (**a**) Schematic drawing of a metal film with a periodic array of holes. The coordinate axes x, y, and z are always directed along the principal axes of the simple square lattice, and the applied static magnetic field **B** always lies in the film plane. The incident light beam is normal to the film surface, i.e., the *ac* electric field **E** is parallel to the film plane, while the wavevector is normal to the film plane (i.e., $\boldsymbol{k} \parallel y$). Note that the *ac* magnetic field **H** of the light wave (**H**⊥**E**) is not important in our considerations and we omit it everywhere. Inset shows an $a \times a$ unit cell of the periodic composite film with a cylindrical hole of radius R at its center. (**b**) The same as in (**a**) but both **B** and the incident field **E** are rotated *together* in the film plane. Here we show the case of the transverse polarization $\mathbf{E} \parallel x' \perp \mathbf{B} \parallel z'$, denoted in the text as ⊥. The longitudinal polarization $\mathbf{E} \parallel \mathbf{B} \parallel z'$ is denoted in the text as ∥. After Ref. [10]

at the sample surface evolves into a refracted wave and a reflected wave. If $\varepsilon_{zy} = \varepsilon_{yz} = 0$, we have

$$N_{\pm}^2 \equiv \left(\frac{c}{\omega}\right)^2 k_{\pm}^2 = \frac{\varepsilon_{xx} + \varepsilon_{yy}}{2} \pm \sqrt{(\frac{\varepsilon_{xx} - \varepsilon_{yy}}{2})^2 \pm \varepsilon_{xy}\varepsilon_{yx}}. \tag{1.4}$$

The refracted beam becomes elliptically polarized with the major axis rotated by the (Faraday) angle [48–56] ϑ_F:

$$\vartheta_F \equiv \frac{1}{2}\left(\frac{\omega l}{c}\right) \mathrm{Re}(N_+ - N_-). \tag{1.5}$$

The expression for the *ellipticity* (the ratio of minor to major axis) e_F can be found in Refs. [48–56]. The reflected beam is also elliptically polarized with ellipticity e_K and the major axis rotated by an angle ϑ_K, similar to the refracted wave (see Refs. [48–56]).

When $\varepsilon_{xx} = \varepsilon_{yy}$ and $\varepsilon_{yx} = -\varepsilon_{xy}$, (1.1) and (1.4) are simplified to the form of right-handed and left-handed elliptically polarized waves $k^2 E_{0\pm} = (\omega/c)^2 \varepsilon_{\pm} E_{0\pm}$, and $N_{\pm}^2 = \varepsilon_{xx} \pm i\varepsilon_{xy}$, respectively. Here $E_{0\pm} = E_{0x} \pm i E_{0y}$, and $\varepsilon_{\pm} = \varepsilon_{xx} \pm i\varepsilon_{xy}$. Equation (1.5) then takes the form $\vartheta_F = \nu B l$, where B is the external applied magnetic field (in Tesla) in the direction of propagation, l is the length of the path (in meters) over which the light and the magnetic field interact, ν is the Verdet constant of the material.

In addition to the longitudinal or Faraday configuration, in which the wave propagates through the sample along the applied magnetic field **B**, there is also the so-called Voigt configuration, in which **B** is perpendicular to the direction of the wave propagation, $k \parallel y$ and $B \parallel z$. The latter case is convenient for demonstrating how important additional off-diagonal terms of the permittivity tensor can be in the case

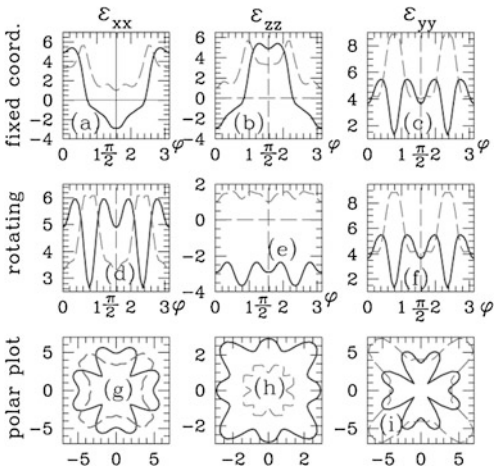

Fig. 1.2 Real (*solid lines*) and imaginary (*dashed lines*) parts of the diagonal components ε_{xx}, ε_{zz}, and ε_{yy} [in the fixed non-rotating (**a**)–(**c**) and rotating (**d**)–(**f**) coordinate systems] of the macroscopic permittivity tensor $\hat{\varepsilon}$ of the metamaterial, made of a simple-square array (with the lattice constant a) of cylindrical circular holes (of radius $R = 0.3a$) in the metallic film. (**a**)–(**c**) ε_{xx}, ε_{zz},and ε_{yy}, plotted vs. the rotation angle ϕ of Fig. 1.1(b), but where these components are taken along the *fixed* coordinates x, y, z of Figs. 1.1(a) and (b). (**d**)–(**f**) Similar to panels (**a**)–(**c**), but now the components of $\hat{\varepsilon}$ are taken along the *rotating* coordinates x', y, z' of Fig. 1.1(b). (**g**)–(**i**) polar plots of (**d**)–(**f**). The permittivity tensor is taken in the quasi-static approximation $\hat{\varepsilon} = \hat{\varepsilon}_0 + i4\pi\hat{\sigma}/\omega$, where $\hat{\sigma}$ is the conductivity tensor of the metal taken in the Drude form with the plasma frequency ω_p and the electron relaxation time τ is such that $\omega_p\tau = 20$. The light frequency is $\omega = 0.4\omega_p$

of metamaterials and why the formulas for MO effects should be expressed in a general form.

If **B** has an arbitrary direction with respect to the lattice axes of the metamaterial, all components of the permittivity tensor can be nonzero [7–12]. When both **B** and **E** are rotated in the film plane, the angular profiles of $\hat{\varepsilon}$ and the optical transmission coefficients $T_\perp$ and $T_\parallel$ are anisotropic (see Ref. [10]). The angular profiles of the diagonal components ε_{xx}, ε_{yy}, ε_{zz}, and the off-diagonal tensor components ε_{xy}, ε_{xz}, ε_{yx}, ε_{yz}, ε_{zx}, and ε_{zy} in non-rotating and rotating coordinate systems are shown in Figs. 1.2 and 1.3. The general expressions for the Faraday rotation and Voigt effect are cumbersome [57]. However, when $\mathbf{B} \parallel z$ is directed along the main lattice axes, some of the permittivity tensor components vanish ($\varepsilon_{xz} = \varepsilon_{yz} = \varepsilon_{zx} = \varepsilon_{zy} = 0$) and general formulas simplify. Equation (1.3) then takes the form

$$N_\perp^2 \equiv \left(\frac{\omega}{c}\right)^2 k_\perp^2 = \varepsilon_{xx} - \frac{\varepsilon_{xy}\varepsilon_{yx}}{\varepsilon_{yy}}, \quad \text{for } E \perp B,$$
$$N_\parallel^2 \equiv \left(\frac{\omega}{c}\right)^2 k_\parallel^2 = \varepsilon_{zz}, \quad \text{for } E \parallel B. \tag{1.6}$$

The Voigt effect, which is also known as the Cotton–Mouton effect, is magnetic birefringence. It is caused by the difference between the transverse, $n_\perp$, and longi-

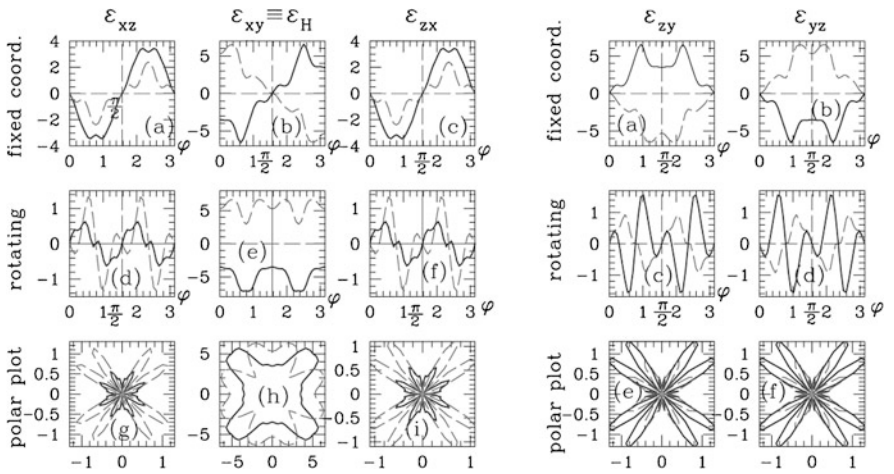

Fig. 1.3 The *left part* is similar to Fig. 1.2, with the off-diagonal components, ε_{xz}, $\varepsilon_{xy}\equiv\varepsilon_H$, and ε_{zx}, taken in fixed non-rotating (**a**)–(**c**) and rotating (**d**)–(**f**) coordinate systems. The component $\varepsilon_{xy}\equiv\varepsilon_H$ of the permittivity tensor is the Hall component. In the polar plots (**g**)–(**i**), the absolute values of the above quantities are shown. The *right part* is similar to the left part, but for the off-diagonal components, ε_{zy}, and ε_{yz}

tudinal, $n_\parallel$, components of $N_{\perp,\parallel}=n_{\perp,\parallel}+i\kappa_{\perp,\parallel}$, where κ is the *absorption index*. The Voigt phase shift δ is given by

$$\delta=\frac{\omega l}{c}(n_\parallel-n_\perp), \tag{1.7}$$

where l is the length of the path.

Assuming that $\omega l/c\sim 1$ and using (1.7) and values of the permittivity tensor $\hat{\varepsilon}$ components shown in Figs. 1.2 and 1.3, we can estimate and compare the values of δ in the (001)- and (011)-directions when $\varepsilon_{xz}=\varepsilon_{yz}=\varepsilon_{zx}=\varepsilon_{zy}=0$. For arbitrary directions, (1.7) would have a much more complicated form. For the values of $\hat{\varepsilon}$ shown in Figs. 1.2 and 1.3, $\delta\sim-0.03$ in the (001)-direction, while in the (011)-direction, $\delta\sim 0.02$. Thus, it is possible to observe the magneto-induced angular anisotropy of δ in periodic metamaterials. The angular anisotropy of other MO effects can be considered similarly.

1.3 Longitudinal Configuration: Enhancement of Magneto-Optical Effects in Gyrotropic Photonic Metamaterials

In order to be consistent with our previous publications [4, 58–61], for the further consideration we denote diagonal and off-diagonal components of the permittivity tensor as ε and g, respectively. For the longitudinal configuration, when the wave

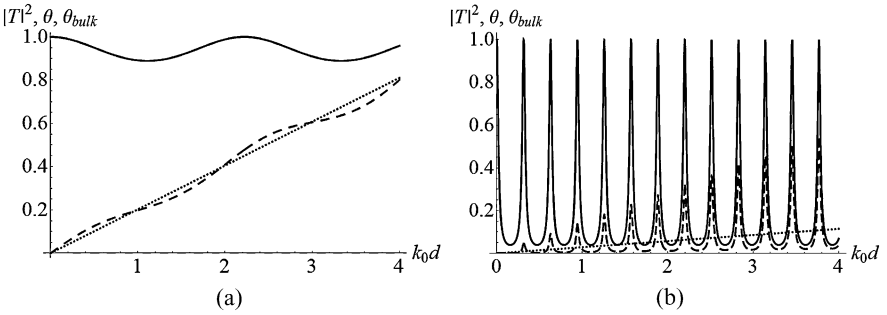

Fig. 1.4 The transmission (*solid lines*), the angle of rotation of the polarization plane ϑ by a slab (*dashed lines*), and the bulk angle of rotation ϑ_{bulk} (*dotted lines*) as a function of frequency k_0 normalized by the thickness of layer d for the parameters (**a**) $\varepsilon = 2$, $g = 0.01$ and (**b**) $\varepsilon = 100$, $g = 0.07$. The external medium is vacuum

travels along the direction of the static magnetic field, (1.5) and (1.6) for the angle of rotation due to smallness of g may be expressed as (see for review [41, 62] and references therein)

$$\vartheta_{\text{bulk}} = \frac{1}{2}\frac{\omega}{c} d(\sqrt{\varepsilon + g} - \sqrt{\varepsilon - g}) \approx \frac{1}{2}\frac{\omega}{c} d\sqrt{\varepsilon}\frac{g}{\varepsilon} = \frac{g}{2\varepsilon} k_{\text{MO}} d_{\text{MO}}, \tag{1.8}$$

where d_{MO} is the light path, $k_{\text{MO}} = k_0\sqrt{\varepsilon}$, and $k_0 = \omega/c$ is the free space wavenumber.

Let us continue with the consideration of the Faraday effect observed in a single homogeneous layer. This example clearly shows the difference between Faraday effects in bulk and bounded systems.

If the magnetized slab has permittivity of the order of unity, the reflected wave is weak, and the Faraday effect is close to its bulk value (see Fig. 1.4(a)). In the case of high permittivity, multiple reflections inside the slab cause sharp Fabry–Pérot resonances in the transmission at the frequencies $\omega_n/c = \pi n/d\sqrt{\varepsilon}$ (where n is an integer). The reflections also modify the Faraday rotation, which is enhanced in the vicinity of resonances and suppressed far from them (see Fig. 1.4(b)).

When the slab is magnetized, the waves with left and right circular polarizations have slightly different wavenumbers. As a result, the transmission maxima are observed at different frequencies

$$\frac{\omega_r^{\pm}}{c} = \frac{\pi n}{d\sqrt{\varepsilon \pm g}}, \tag{1.9}$$

where "+" and "−" indicate right and left polarizations, respectively. A splitting of the circular polarizations similar to (1.9) appears in the case of normal incidence for any multilayered structure, containing MO layers and producing a resonance (see the next section). The enhancement of the Faraday effect is due to general properties of the resonance; therefore, below a general case is considered.

The frequency dependences of phase $\phi(k_0)$ and transmittance $T(k_0)$ near a MO-split resonance for the right and left polarizations are shown in Fig. 1.5 by the dashed

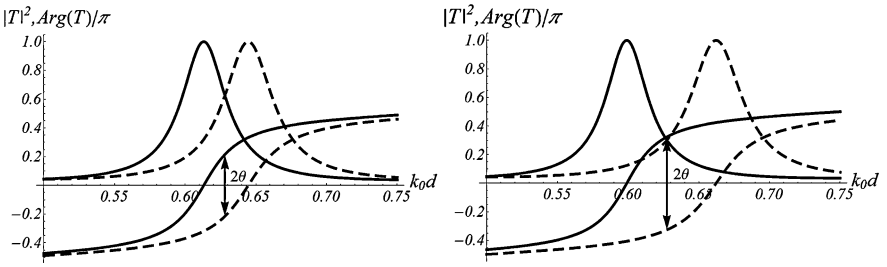

Fig. 1.5 The amplitude and the argument of the transmission coefficient for the case of nonzero magnetization. (**a**) $\varepsilon = 100$, $g = 5$, and (**b**) $\varepsilon = 100$, $g = 10$. The value of g is taken large enough to make the splitting visible

and solid lines, respectively. Disregarding the deformation of curves, one can express these dependences for the left and right circular polarizations as

$$\begin{aligned} &\varphi^+(\omega) = \varphi(\omega + 0.5\Delta\omega_r) \quad \text{and} \quad \varphi^-(\omega) = \varphi(\omega - 0.5\Delta\omega_r), \\ &\left|T^+(\omega)\right|^2 = \left|T(\omega + 0.5\Delta\omega_r)\right|^2 \quad \text{and} \quad \left|T^-(\omega)\right|^2 = \left|T(\omega - 0.5\Delta\omega_r)\right|^2, \end{aligned} \tag{1.10}$$

where $\varphi(\omega)$, $|T(\omega)|^2$ are the dependences at zero magnetization, $\Delta\omega_r = \omega_r^+ - \omega_r^-$. The angle of the Faraday rotation is equal to [41]

$$\vartheta = 0.5\big(\varphi^+(\omega) - \varphi^-(\omega)\big). \tag{1.11}$$

It is obvious from Fig. 1.5 that the enhancement is due to the fast growth of the phase, which changes by π on the scale of the resonant line width. Note that instead of the small bulk value (1.8) one can obtain the Faraday angle of the order of $\pi/2$, which follows from the fact that the phase changes by π in the vicinity of any resonance and from the formula (1.11).

The transmitted wave is linearly polarized at the frequency ω^*, defined by the condition

$$\left|T^+\big(\omega^*\big)\right|^2 = \left|T^-\big(\omega^*\big)\right|^2 \tag{1.12}$$

(we imply that the incident wave is linearly polarized). Taking into account a single resonance only, the value of ω^* is evaluated as

$$\omega^* = 0.5\big(\omega_r^- + \omega_r^+\big) = \omega_r, \tag{1.13}$$

i.e., ω^* is equal to the resonant frequency of non-magnetized system.

It is essential that the enhancement of the Faraday rotation is observed when the condition (1.13) is fulfilled, or, at least, the frequency lies between the split resonance frequencies. Suppose that the Q-factors of "+" and "−" resonances significantly differ (Fig. 1.6). There exist two points satisfying the condition (1.12). The number of paths the light makes traveling through the system is the same but the Faraday rotation is different. Comparison of Figs. 1.5 and 1.6 shows that it is important that $\omega_r^+ < \omega^* < \omega_r^-$.

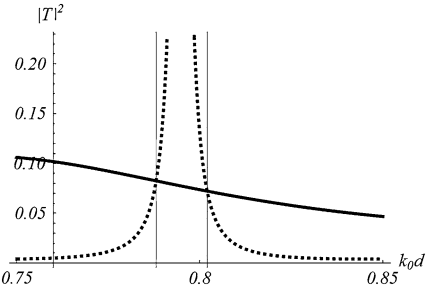

Fig. 1.6 Two resonances for different Q-factors

The smaller the MO splitting the higher transmittance (1.12) and smaller the Faraday rotation (Figs. 1.5(a) and (b)). It can be shown (see [36] and Appendix A) that

$$T = T_0 \cos^2 \vartheta \tag{1.14}$$

where T_0 is a transmittance at zero magnetization. When ϑ increases, the rotation angle saturates at the value of $\pi/2$. At the same time, the amplitude of the transmitted wave tends to zero.

Usually, the splitting $\Delta\omega_r$ is much smaller than the resonance width. Then the Faraday rotation angle, according to (1.10) and (1.11), can be estimated as

$$\begin{aligned}\vartheta(\omega_r) &= \frac{1}{2}\left[\varphi\left(\omega_r^- + \Delta\omega_r/2\right) - \varphi\left(\omega_r^+ - \Delta\omega_r/2\right)\right] \approx \frac{1}{2}\left.\frac{d\varphi(\omega)}{d\omega}\right|_{\omega=\omega_r} \Delta\omega_r \\ &= \left.\frac{d\varphi(\omega)}{d\omega}\right|_{\omega=\omega_r} \frac{\partial\omega_r}{\partial\varepsilon} g. \end{aligned} \tag{1.15}$$

According to (1.15), $\vartheta(\omega_r)$ is determined by three factors. The first one, $d\varphi(\omega)/d\omega|_{\omega=\omega_r}$, is equal to the inverse width of the resonance $1/\Gamma$ (see Appendix B). The second factor, $\partial\omega_r/\partial\varepsilon$, is the sensitivity of the resonance position to the value of the dielectric constant of the MO layers. Note that this parameter is not related to MO properties of the slab. If the structure is a uniform MO slab of the width d, one has

$$\omega_r = \frac{\pi n}{d\sqrt{\varepsilon}} \quad \text{and} \quad \frac{\partial\omega_r}{\partial\varepsilon} = -\omega_r \frac{1}{2\varepsilon},$$

from which we obtain

$$\vartheta \approx -\frac{1}{\Gamma}\omega_r \frac{g}{2\varepsilon} = -Q\frac{g}{\varepsilon} \tag{1.16}$$

where $\omega_r/2\Gamma = Q$ is the Q-factor of the resonance. In the general case of arbitrary multilayer structure, (1.16) can be rewritten as

$$\vartheta \approx \frac{1}{\Gamma}\omega_r \frac{g}{\varepsilon}\frac{\partial \ln\omega_r}{\partial \ln\varepsilon} = Q\frac{g}{\varepsilon}2\frac{\partial \ln\omega_r}{\partial \ln\varepsilon}, \tag{1.17}$$

where the derivative corresponds to the shift of the resonance frequency with the change of the permittivity of the MO layers. One can show that

$$-\frac{1}{2} \le \frac{\partial \ln\omega_r}{\partial \ln\varepsilon} \le 0.$$

For closed resonators (with infinite Q-factor) the shift of the resonance frequency with the change of permittivity is determined by the expression [63]:

$$\frac{\partial \ln \omega_r}{\partial \ln \varepsilon} \approx -\frac{1}{2} \frac{\int_{\mathrm{MO}} \varepsilon |E|^2 \, dz}{\int_{\mathrm{res}} \varepsilon |E|^2 \, dz} \tag{1.18}$$

where the integrals in the numerator and the denominator are calculated over the MO layers (their permittivity changes) and over the whole resonance structure, respectively. The latter expression can approximately be applied to a high-Q cavity, such as a finite PC with defect. According to (1.18), the value of $-2\frac{\partial \ln \omega_r}{\partial \ln \varepsilon}$ is approximately equal to the fraction of the energy of the electric field localized in the MO layers. The numerical calculations for the optical Tamm state give $\frac{\partial \ln \omega_r}{\partial \ln \varepsilon} = -0.1786$, which is close to the value given by (1.18)

$$-\frac{1}{2} \frac{\int_{\mathrm{MO}} \varepsilon |E|^2 \, dz}{\int_{\mathrm{res}} \varepsilon |E|^2 \, dz} = -0.1793.$$

Thus, we obtain a simple expression for the resonantly enhanced Faraday rotation:

$$\vartheta \approx -QW\frac{g}{\varepsilon}, \tag{1.19}$$

where

$$W = \frac{\int_{\mathrm{MO}} \varepsilon |E|^2 \, dz}{\int_{\mathrm{res}} \varepsilon |E|^2 \, dz}$$

is the confinement factor [64] and Q is the quality factor of the resonance. It follows from (1.19) that the rotation angle depends not only on the relative concentration of the electric field in MO layers, but also on the total quality factor of the resonance structure. In particular, some decrease in $|\frac{\partial \ln \omega_r}{\partial \ln \varepsilon}|$ can be justified by significant increase in Q. This is the case when multilayered structures are used instead of a single homogeneous MO layer.

1.4 Employing Magnetophotonic Crystals to Enhance the Faraday Effect

Enhancement of the Faraday effect requires a high Q-factor. In the case of a single homogeneous MO layer, in order to achieve a high Q-factor, it is necessary to have an exceedingly large permittivity value. Therefore, more complicated structures should be used, e.g., photonic crystals with defects [35, 65], coupled photonic crystals with optical Tamm states [5, 6, 16], random systems [44], etc.

The simplest structure is a MO layer (defect) placed inside of a bounded PC sample. The working frequency is placed inside the PC's bandgap. If considering two pieces of PC sandwiching the MO-defect as dielectric mirrors, the structure looks like a common Fabry–Pérot resonator, where the resonant frequency is equal to the frequency of the defect mode [66] localized at the defect.

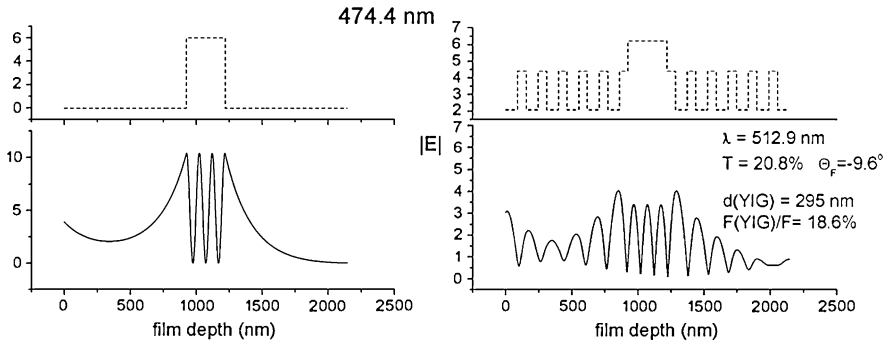

Fig. 1.7 Permittivity (*top figures*) and field distribution (*bottom figures*) in a cavity with (**a**) homogeneous (low-permittivity) mirrors and (**b**) layered mirrors (a PC with bandgap)

The benefits of employing a MPC instead of metallic mirrors originate from possibility of increasing the Q-factor by the redistribution of the light energy from materials with losses into low loss materials [6]. Due to the complicated structure of the Bloch wave, an exponential decay in the bandgap happens only on average. Locally, the field may achieve high values (Fig. 1.7). Thus, a significant part of the energy may be concentrated in low-loss dielectric mirrors instead of lossy defect. This leads to increase of the Q-factor.

Instead of the defect mode one can use the surface Tamm state appearing in between two PCs. In this case, there is no cavity, and the field is located inside the PC-mirrors, incorporating MO layers.

The Faraday rotation can be enhanced by employing the Borrmann effect [64]. This effect is related to the fact that for a frequency of band edge, the Bloch wave is a standing wave whose maxima lie either in the higher- or in the lower-permittivity layers [67]. In such a way, the energy of the electric field can be concentrated in the MO layers, thereby increasing the confinement factor W.

Using a single resonance, one can obtain any value of the Faraday rotation angle up to 90°. However, it is accompanied by inevitable decrease in the signal amplitude (see (1.14) and [36]). Using two resonances [36], one can have the 90° Faraday rotation at $T = 1$, overcoming the limit, expressed by (1.14). So, let us now consider the case when the splitting of the resonance Δk_r is equal to the distance between neighboring resonances. This can be achieved either by using a structure with two defects [36, 37], or by choosing a defect-free MPC with sufficiently large number of layers. In this case, the resonances of different orders, $T_n^+(k_0)$ and $T_{n-1}^-(k_0)$, overlap, as shown in Fig. 1.8(a). Since each resonance causes a change of the phase by π, the phase difference between two polarizations is also π (see Fig. 1.8(b) and 7 at $k_0 L = 11.58$). Thus, the angle of the Faraday rotation is equal to $\pi/2$, whereas the coincidence of resonances for both polarizations leads to transmission equal to unity (Fig. 1.9).

For a practical realization of this situation with existing MO materials, different resonances must be close to each other. This can be achieved by increasing the number of layers in a PC and using a wavenumber that is close to a bandedge. The

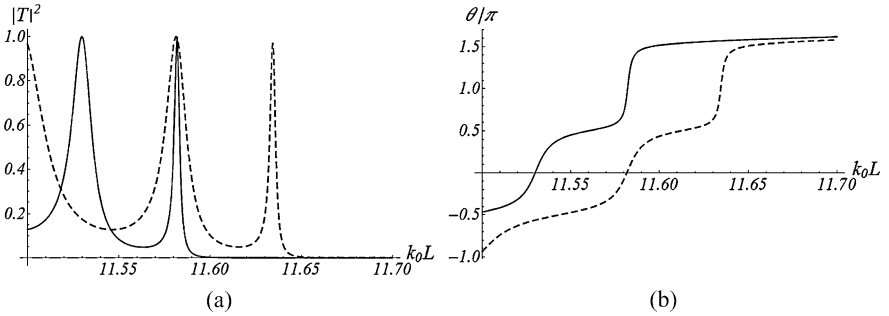

(a) (b)

Fig. 1.8 The transmission coefficient (**a**) and the phase shift (**b**) in the case when resonances of different order coincide. *Solid* and *dashed lines* correspond to the right and left polarizations, respectively. The elementary cell of the PC consists of two layers with parameters $\varepsilon_1 = 1$, $d_1 = 0.1$ μm, $\varepsilon_2 = 2$, $g = 0.01$, and $d_2 = 0.1$ μm. The total number of layers is 58

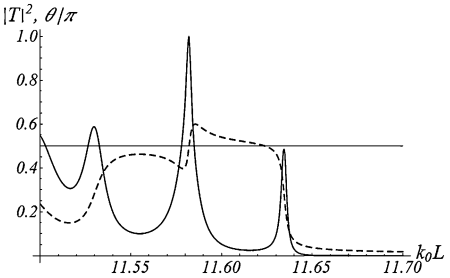

Fig. 1.9 The transmission (*solid line*) and the angle of rotation of the polarization plane (*dashed line*) for a sample with parameters described in Fig. 1.8

density of the resonances is proportional to the density of states (inversely proportional to the group velocity) that has a maximum at the bandedge. An increase in the number of layers allows one to make the density of states arbitrarily large. This makes the transmission resonances dense enough.

To conclude it is worth mentioning some systems, employing plasmon resonance for enhancement of the Faraday effect. In these systems, the property of surface plasmon to have given (*TM*) polarization is used [68, 69]. The obliquely incident *TE*-polarized wave in the frustrated total internal reflection geometry (Fig. 1.10(a)) does not excite a surface plasmon at the metal/dielectric interface, if the magnetization is zero. However, in the presence of magnetization, there arises an interaction between the *TE* and *TM* polarizations, and the generation of *TM*-polarized surface plasmon enhances the cross-polarization. Thus, the scheme in Fig. 1.10(a) transforms a *TE*-polarized wave into *TM*-polarized wave producing an effective rotation of the polarization plane by $\pi/2$. At the same time, the intensity of the transmitted wave is low. The effectiveness of the plasmonic scheme can be compared to the one of the usual schemes, discussed above, by calculating the cross-polarization intensity in the usual schemes. It is easy to see from (1.12) that in the usual scheme the cross-polarization intensity, which is proportional to the square of ϑ, grows with the quality factor as Q^2. In the plasmonic scheme, it depends on Q logarithmically, which in fact reduces the enhancement to nothing. The reason for such dependence

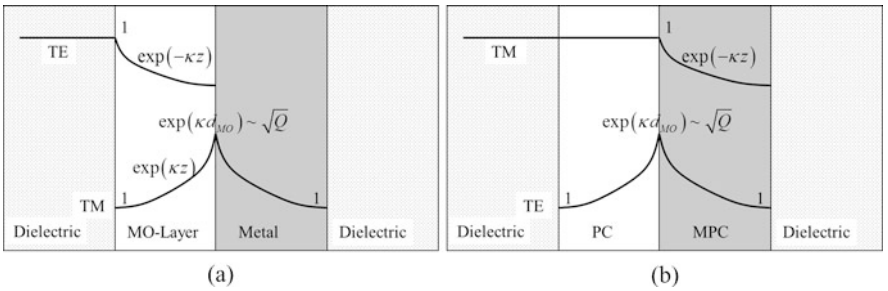

Fig. 1.10 Plasmonic enhancement of the Faraday rotation. (**a**) The original scheme [68], providing the logarithmic in Q-factor enhancement of the cross-polarization intensity. (**b**) Modified scheme providing the linear in Q-factor enhancement of the cross-polarization intensity (the Bloch wave envelope is shown)

is the weak interaction between the incident wave and the one having the perpendicular polarization. This interaction is proportional to the overlap of the *TE*- and *TM*-polarized fields in the MO layer (Fig. 1.10(a)).

The overlap can be increased, if the surface wave at the PC/MPC interface (Fig. 1.10(b)) is used instead of the surface plasmon at the interface of the homogeneous medium. In this case, the wave of *TM* polarization should reach the PC/MPC interface without decay, and only in the MPC it should become evanescent due to the bandgap. MO layers create the cross-(*TE*) polarization, which decays in both the PC and MPC due to the bandgap. The conditions for existence of the *TE*-polarized surface wave at the PC/MPC interface should be satisfied, which results in the cross-polarization enhancement. It turns out that all these conditions are easily satisfied if: (1) the angle of incidence ensures the Brewster condition for the layers of the PC; (2) all the layers are quarter-wavelength ones at the given angle. The overlap of the fields in the MO layers (Fig. 1.10(b)) is now increased, leading to the cross-polarization intensity being proportional to the Q-factor. However, even this scheme is not as good as the usual one, working at normal incidence. The reason is that the resonance in the usual schemes amplifies not only the cross-polarization, but also the incident one. Since the cross-polarization is created by the incident wave, it undergoes quadratic in Q amplification. The schemes amplifying only the cross-polarization cannot give more than a linear dependence.

1.5 Conclusions

In this chapter, we develop a general approach for considering structures used for the Faraday effect enhancement. These structures can be considered as open resonators in which bulk MO properties remove the degeneracy with respect to the polarization and split the resonance frequencies. At the frequency in-between the frequencies of the split resonance, a large rotation of the polarization plane can be observed. This rotation is due to the rapid change of the phase of the transmitted wave by a value

of π when the frequency of the incident wave crosses the resonance. Indeed, at these frequencies, the phase of the red shifted wave gains a value of the order of π, while the phase of the blue shifted wave hardly changes. When the splitting is much smaller than the resonance width, the Faraday rotation is shown to be a product of the resonance Q-factor, confinement factor and the MO factor.

Appendix A: Relationship Between the Transmission Coefficient and the Faraday Rotation Angle

We assume that the distance between a given resonance and other ones is much larger than the resonance width. In principle, if the resonance has a large Q-factor, a small magnetization is sufficient for obtaining the required value of splitting of resonances. But, irrespective of the Q-factor, one obtains the same dependence of the transmission coefficient $|T|^2$ on the Faraday rotation angle ϑ (Fig. 1.11). This is due to the fact that the frequency range in the vicinity of the resonance, at which the amplitude, $|T|^2$, and the phase, $\arg T$, change significantly, is the same for both these quantities. More precisely, for $T(k_0) = \frac{\alpha}{k_0 - \tilde{k}_0}$ with a real frequency, k_0, and complex values of residue, α, and the pole position, $\tilde{k}_0 = k_r - i\Gamma$, one can obtain the expression $|T|^2 = T_0^2 \cos^2 \vartheta$ (T_0^2 is the resonant transmission), which is independent of the Q-factor. Indeed, designating a deviation of the frequency from the resonant one as $\delta k_0 = k_0 - k_r$, one has $T(\delta k_0) = \frac{\alpha}{\delta k_0 + i\Gamma}$ and

$$\left|T(\delta k_0)\right|^2 = \frac{|\alpha|^2}{\delta k_0^2 + \Gamma^2}. \tag{1.20}$$

Presuming that the presence of the magnetization shifts the peak without changing its form, one obtains $\vartheta = (\arg T(\delta k_0) - \arg T(-\delta k_0))/2$, from which it follows that

$$\tan \vartheta = -\frac{\delta k_0}{\Gamma}. \tag{1.21}$$

Eliminating δk_0 from expressions (1.20) and (1.21), one obtains $|T|^2 = \frac{|\alpha|^2}{\Gamma^2} \cos^2 \vartheta$. After denoting the transmission at the resonance as $T_0^2 = \frac{|\alpha|^2}{\Gamma^2}$, the required result arises:

$$|T|^2 = T_0^2 \cos^2 \vartheta. \tag{1.22}$$

The comparison between the one-resonance model system meeting condition (1.22) and results obtained from calculations of the Tamm state (Fig. 1.11) shows that a difference appears when the frequency moves away from the resonance, to the region in which the resonances next to the Tamm state become visible.

From this analysis one can conclude that for any lossless system with separated resonances, a large rotation angle is possible only for a small transmission, and their mutual dependence is the same for any Q-factor. A large Q-factor is needed only for obtaining the desirable value of splitting of peaks which is equal to $2\delta k_0$.

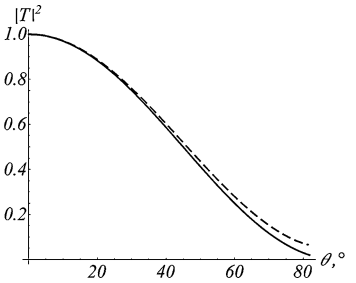

Fig. 1.11 Universal dependence of the transmission coefficient on the Faraday rotation angle for a single pole (*solid line*) and the same dependence for the optical Tamm state resonance (*dashed line*). The deviation is caused by resonances neighboring to the Tamm state

Appendix B: Rate of the Phase Change at the Resonance Frequency

In this appendix we show that at the resonance, the absolute value of the quantity $d\varphi/d\omega|_{\omega=\omega_r}$ in (1.15), is equal to the inverse width of the resonance. Near the resonance, the transfer function can be approximated as

$$T(\omega) = \frac{\alpha}{\omega - \omega_r - i\Gamma},$$

where ω_r and Γ are the frequency and the half-width of the resonance, respectively. By differentiating the relation $T(\omega) = |T(\omega)| \exp(i\varphi(\omega))$, one obtains

$$\frac{\partial\varphi}{\partial\omega} = \frac{i}{|T|}\frac{\partial|T|}{\partial\omega} - \frac{i}{T}\frac{\partial T}{\partial\omega}.$$

Calculating derivatives

$$\frac{\partial|T|}{\partial\omega} = \frac{\partial}{\partial k}\frac{|\alpha|}{\sqrt{(\omega-\omega_r)^2+\Gamma^2}} = -|T|\frac{\omega-\omega_r}{(\omega-\omega_r)^2+\Gamma^2}$$

and

$$\frac{\partial T}{\partial\omega} = -\frac{T}{\omega-\omega_r-i\Gamma},$$

we find

$$\frac{\partial\varphi}{\partial\omega} = -\frac{\Gamma}{(\omega-\omega_r)^2+\Gamma^2}.$$

It immediately follows that at the resonance

$$\frac{d\varphi(\omega)}{d\omega} = -\frac{1}{\Gamma}.$$

References

1. H. Raether, *Surface Plasmons on Smooth and Rough Surfaces and on Gratings* (Springer, Berlin, 1988)

2. T.W. Ebbesen, H.J. Lezec, H.F. Ghaemi, T. Thio, P.A. Wolff, Nature **391**, 667–669 (1998)
3. C. Genet, T.W. Ebbesen, Nature **445**, 39–46 (2007)
4. T. Goto, A.V. Dorofeenko, A.M. Merzlikin, A.V. Baryshev, A.P. Vinogradov, M. Inoue, A.A. Lisyansky, A.B. Granovsky, Phys. Rev. Lett. **101**, 113902 (2008)
5. A.P. Vinogradov, A.V. Dorofeenko, S.G. Erokhin, M. Inoue, A.A. Lisyansky, A.M. Merzlikin, A.B. Granovsky, Phys. Rev. B **74**, 045128 (2006)
6. A.P. Vinogradov, S.G. Erokhin, A. Granovsky, M. Inoue, J. Commun. Technol. Electron. **49**, 88 (2004)
7. D.J. Bergman, Y.M. Strelniker, Phys. Rev. Lett. **80**, 857–860 (1998)
8. Y. Fleger, M. Rosenbluh, Y.M. Strelniker, D.J. Bergman, A.N. Lagarkov, Eur. Phys. J. B **81**, 85–93 (2011)
9. Y.M. Strelniker, Phys. Rev. B **76**, 085409 (2007)
10. Y.M. Strelniker, D.J. Bergman, Phys. Rev. B **59**, R12763–R12766 (1999)
11. Y.M. Strelniker, D.J. Bergman, Phys. Rev. B **77**, 205113 (2008)
12. Y.M. Strelniker, D. Stroud, A.O. Voznesenskaya, Eur. Phys. J. B **52**, 1–7 (2006)
13. N. Ou, J.H. Shyu, J.C. Wu, T.H. Wu, IEEE Trans. Magn. **45**, 4027–4029 (2009)
14. S. Erokhin, L. Deych, A. Lisyansky, A. Granovsky, Tech. Phys. Lett. **35**, 785–788 (2009)
15. A. Merzlikin, A. Vinogradov, M. Inoue, A. Granovsky, Phys. Solid State **50**, 873–877 (2008)
16. A.M. Merzlikin, A.P. Vinogradov, A.V. Dorofeenko, M. Inoue, M. Levy, A.B. Granovsky, Physica B, Condens. Matter **394**, 277–280 (2007)
17. A.M. Merzlikin, A.P. Vinogradov, M. Inoue, A.B. Khanikaev, A.B. Granovsky, J. Magn. Magn. Mater. **300**, 108–111 (2006)
18. V. Belotelov, D. Bykov, L. Doskolovich, A. Kalish, A. Zvezdin, Phys. Solid State **51**, 1656–1662 (2009)
19. V.I. Belotelov, L.L. Doskolovich, V.A. Kotov, E.A. Bezus, D.A. Bykov, A.K. Zvezdin, Opt. Commun. **278**, 104–109 (2007)
20. A.B. Khanikaev, A.V. Baryshev, A.A. Fedyanin, A.B. Granovsky, M. Inoue, Opt. Express **15**, 6612–6622 (2007)
21. V.G. Kravets, A.S. Lapchuk, Appl. Opt. **49**, 5013–5019 (2010)
22. A. García-Martín, G. Armelles, S. Pereira, Phys. Rev. B **71**, 205116 (2005)
23. B. Sepúlveda, L.M. Lechuga, G. Armelles, J. Lightwave Technol. **24**, 945 (2006)
24. L.E. Helseth, Phys. Rev. B **72**, 033409 (2005)
25. A. Battula, S. Chen, Y. Lu, R.J. Knize, K. Reinhardt, Opt. Lett. **32**, 2692–2694 (2007)
26. G.A. Wurtz, W. Hendren, R. Pollard, R. Atkinson, L.L. Guyader, A. Kirilyuk, R. Th, I.I. Smolyaninov, A.V. Zayats, New J. Phys. **10**, 105012 (2008)
27. G. Armelles, J.B. González-Díaz, A. García-Martín, J.M. García-Martín, A. Cebollada, M.U. González, S. Acimovic, J. Cesario, R. Quidant, G. Badenes, Opt. Express **16**, 16104–16112 (2008)
28. J. Han, A. Lakhtakia, Z. Tian, X. Lu, W. Zhang, Opt. Lett. **34**, 1465–1467 (2009)
29. R. Zhou, H. Li, B. Zhou, L. Wu, X. Liu, Y. Gao, Solid State Commun. **149**, 657–661 (2009)
30. J.H. Kang, Q.H. Park, D.S. Kim, J. Korean Phys. Soc. **55**, 1295 (2009)
31. B. Hu, B.-Y. Gu, Y. Zhang, M. Liu, Appl. Phys. Lett. **95**, 121103 (2009)
32. C. Clavero, K. Yang, J.R. Skuza, R.A. Lukaszew, Opt. Express **18**, 7743–7752 (2010)
33. D.M. Newman, M.L. Wears, R.J. Matelon, Europhys. Lett. **68**, 692 (2004)
34. M. Kohmoto, B. Sutherland, K. Iguchi, Phys. Rev. Lett. **58**, 2436–2438 (1987)
35. M. Inoue, T. Fujii, J. Appl. Phys. **81**, 5659–5661 (1997)
36. M.J. Steel, M. Levy, R.M. Osgood, J. Lightwave Technol. **18**, 1297 (2000)
37. S. Sakaguchi, N. Sugimoto, J. Lightwave Technol. **17**, 1087–1092 (1999)
38. H. Shimizu, M. Miyamura, M. Tanaka, Appl. Phys. Lett. **78**, 1523–1525 (2001)
39. H. Kato, T. Matsushita, A. Takayama, M. Egawa, K. Nishimura, M. Inoue, J. Appl. Phys. **93**, 3906–3911 (2003)
40. M. Inoue, K. Arai, T. Fujii, M. Abe, J. Appl. Phys. **85**, 5768–5770 (1999)
41. A.K. Zvezdin, V.A. Kotov, *Modern Magnetooptics and Magnetooptical Materials* (IOP, Bristol, 1997)

42. S. Visnovsky, V. Prosser, R. Krishnan, J. Appl. Phys. **49**, 403–408 (1978)
43. G.S. Krinchik, O.B. Esikova, A.A. Kostyurin, Opt. Spectrosc. **44**, 471–472 (1978)
44. M. Inoue, K. Arai, T. Fujii, M. Abe, J. Appl. Phys. **83**, 6768–6770 (1998)
45. E. Takeda, N. Todoroki, Y. Kitamoto, M. Abe, M. Inoue, T. Fujii, K. Arai, J. Appl. Phys. **87**, 6782–6784 (2000)
46. A.K. Zvezdin, V.I. Belotelov, Eur. Phys. J. B **37**, 479–487 (2004)
47. V.I. Belotelov, L.L. Doskolovich, A.K. Zvezdin, Phys. Rev. Lett. **98**, 077401 (2007)
48. S.D. Smith, in *Light and Matter, Ia, Encyclopedia of Physics*, ed. by L. Genzel (Springer, Berlin, 1967)
49. P.N. Argyres, Phys. Rev. **97**, 334–345 (1955)
50. R. Stevenson, Can. J. Phys. **38**, 941–944 (1960)
51. J.G. Mavroides, in *Properties of Solids*, ed. by F. Abeles (North-Holland, Amsterdam, 1972)
52. F. Abeles, in *Properties of Solids*, ed. by F. Abeles (North-Holland, Amsterdam, 1972)
53. W.J. Tabor, F.S. Chen, J. Appl. Phys. **40**, 2760–2765 (1969)
54. N. Saleh, S. Zukotynski, Phys. Status Solidi (b) **37**, 879–888 (1970)
55. S. Zukotynski, N. Saleh, Phys. Status Solidi (b) **36**, 593–599 (1969)
56. A.V. Sokolov, *Optical Properties of Metals* (Elsevier, New York, 1967)
57. Y.M. Strelniker, D.J. Bergman, A.P. Vinogradov, Physica B (2013, accepted for publication)
58. A.V. Dorofeenko, A.P. Vinogradov, A.M. Merzlikin, A.B. Granovsky, A.A. Lisyansky, Y.E. Lozovik, in *Proceedings of NMMM–21*, Moscow, June 28–July 4 (2009), pp. 206–208
59. S. Erokhin, A. Lisyansky, A. Merzlikin, A. Vinogradov, A. Granovsky, Phys. Solid State **52**, 65–69 (2010)
60. S.G. Erokhin, A.A. Lisyansky, A.M. Merzlikin, A.P. Vinogradov, A.B. Granovsky, Phys. Rev. B **77**, 233102 (2008)
61. T. Goto, A.V. Baryshev, M. Inoue, A.V. Dorofeenko, A.M. Merzlikin, A.P. Vinogradov, A.A. Lisyansky, A.B. Granovsky, Phys. Rev. B **79**, 125103 (2009)
62. J. Stöhr, H.C. Siegmann, *Magnetism: From Fundamentals to Nanoscale Dynamics* (Springer, Berlin, 2006)
63. L.D. Landau, E.M. Lifshitz, L.P. Pitaevskii, in *Electrodynamics of Continuous Media*, (Butterworth-Heinemann, Oxford, 1995)
64. A.P. Vinogradov, Y.E. Lozovik, A.M. Merzlikin, A.V. Dorofeenko, I. Vitebskiy, A. Figotin, A.B. Granovsky, A.A. Lisyansky, Phys. Rev. B **80**, 235106 (2009)
65. M. Inoue, R. Fujikawa, A. Baryshev, A. Khanikaev, P.B. Lim, H. Uchida, O. Aktsipetrov, A. Fedyanin, T. Murzina, A. Granovsky, J. Phys. D, Appl. Phys. **39**, R151 (2006)
66. A. Figotin, V. Gorentsveig, Phys. Rev. B **58**, 180–188 (1998)
67. J.D. Joannopoulos, S.G. Johnson, J.N. Winn, R.D. Meade, *Photonic Crystals: Molding the Flow of Light* (Princeton University Press, Princeton, 2008)
68. V.I. Safarov, V.A. Kosobukin, C. Hermann, G. Lampel, J. Peretti, C. Marlière, Phys. Rev. Lett. **73**, 3584–3587 (1994)
69. N. Richard, A. Dereux, E. Bourillot, T. David, J.P. Goudonnet, F. Scheurer, E. Beaurepaire, J. Appl. Phys. **88**, 2541–2547 (2000)